Improving GEDI Footprint Geolocation Using a High-Resolution Digital Elevation Model

Anouk Schleich, Sylvie Durrieu, Maxime Soma, Cédric Vega

Improving GEDI Footprint Geolocation Using a High-Resolution Digital Elevation Model

Anouk Schleich, Sylvie Durrieu, Maxime Soma, and Cédric Vega

***Abstract*—Global Ecosystem Dynamics Investigation (GEDI) is a lidar system on-board the International Space Station designed to study forest ecosystems. However, GEDI footprint low accuracy geolocation is a major impediment to the optimal benefit of the data. We thus proposed a geolocation correction method, GeoGEDI, only based on high-resolution digital elevation models (DEMs) and GEDI derived ground elevations. For each footprint, an error map between GEDI ground estimates and reference DEM was computed, and a flow accumulation algorithm was used to retrieve the optimal footprint position. GeoGEDI was tested on 150 000 footprints in Landes and Vosges, two French forests with various stands and topographic conditions. It was applied to GEDI versions 1 (v1) and 2 (v2), by either a single or four full-power laser beam tracks. GeoGEDI output accuracy was evaluated by analyzing shift distributions and comparing GEDI ground elevations and surface heights to reference data. GeoGEDI corrections were greater for v1 than for v2 and agreed with errors published by NASA. Within forests, GeoGEDI improved the root mean square error (RMSE) of ground elevation in Landes by 26.8% (0.34 m) and by 13.3% (0.14 m) for v1 and v2, respectively. For Vosges, ground elevation RMSE improved by 59.6% (3.82 m) and 36.2% (1.41 m), for v1 and v2, respectively. Regarding surface heights, except for v2 in Landes, where insufficient variations in topography combined to GEDI ground detection issues might have penalized the adjustment, GeoGEDI improved GEDI estimates. Using GeoGEDI showed efficient to improve positioning bias and precision.**

***Index Terms*—Accuracy, canopy height, digital elevation model (DEM), forest, geolocation, geolocation correction, Global Ecosystem Dynamics Investigation (GEDI), spaceborne lidar.**

I. Introduction

THE Global Ecosystem Dynamics Investigation (GEDI) instrument has been designed to collect unique data on vegetation structure [1]. Launched by NASA in 2018, GEDI is a high-resolution laser system installed onboard the International Space Station (ISS) [2]. Since March 2019, GEDI has been acquiring high-quality 3-D observations over noncontiguous 25 m circular footprints on the ground, between 51.6° North and South latitudes, which have proven highly relevant to the study in forest ecosystems on a global scale [2], [3].

GEDI footprint geolocations are derived from GEDI's own inertial measurement unit, global positioning systems, and star tracker sensors onboard the ISS [2], [4], [5]. However, the ISS's low orbit, size, and shape result in increased mechanical vibrations and greater variations in orientation and altitude than traditional Earth Observation satellites [6]. Consequently, the horizontal position precision of GEDI footprints was expected at 10 m after calibration [2]. For GEDI products' first version (v1), released before in-flight calibration, the mean 1 σ horizontal geolocation error reached 23.8 m. After a calibration process accounting for geolocation biases, a second data (v2) version was released in April 2021 with a positioning error estimated at 10.2 m, with final targeted accuracy at 8 m [4], [7]. Assuming as in [8] that GEDI geolocation errors follow a normal distribution N ($\mu = 0$ m, $\sigma = 10$ m), 68.3%, 78.9%, and 95.4% of the footprints would have a horizontal location error within 10, 12.5, and 20 m, respectively. Owing to footprint diameter on the ground (i.e., 25 m), more than 20% of footprints overlap by less than 50% with the expected footprint. This hampers the comparison and combination between GEDI data and other georeferenced data, such as field measurements and continuous remote sensing data, and therefore GEDI products' qualification and the development of models to predict vegetation attributes from GEDI data [1], [9].

Recent studies assessed GEDI data quality to estimate ground elevation, canopy height, and aboveground biomass (AGB) through comparison with aerial lidar system (ALS) data [10], [11], [12], [13]. GEDI was found to provide accurate ground elevation and canopy top heights measurements, although errors can reach up to several meters [14], [15], [16], [17], [18]. A significant part of errors was attributed to low horizontal accuracy [1], [2], [8], [12], [14], [18]. Based on GEDI data simulations, Milenković et al. [19] showed that AGB estimation errors increase with increasing geolocation error. The geolocation error has more impact in heterogeneous forests and in fragmented land-covers than in very homogeneous forests [8], [19]. Slope and density of canopy cover have shown to influence GEDI estimations [14], [15], [17], [20], [21], but the link with geolocation error impact has not been tested in these studies. However, as

Manuscript received 2 January 2023; revised 27 April 2023; accepted 19 July 2023. Date of publication 26 July 2023; date of current version 29 August 2023. This work was supported in part by the SLIM project, supported by the TOSCA Continental Surface Program of the Centre National d'Etudes Spatiales (CNES) under Grant 4500066524; and in part by the CNES for the Postdoctoral position of Maxime Soma and the cofounding by INRAE and IGN for the Ph.D. thesis of Anouk Schleich. The work of Cédric Vega was supported by Labex ARBRE under Grant ANR-11-LABX-0002-01. *(Corresponding author: Anouk Schleich.)*

Anouk Schleich and Sylvie Durrieu are with the UMR TETIS, Univ Montpellier, AgroParisTech, CIRAD, CNRS, INRAE, F-34196 Montpellier, France (e-mail: anouk.schleich@inrae.fr; sylvie.durrieu@inrae.fr).

Maxime Soma was with the UMR TETIS, Univ Montpellier, AgroParisTech, CIRAD, CNRS, INRAE, F-34196 Montpellier, France. He is now with the UMR RECOVER, INRAE, CS 40061-13182 Aix-en-Provence, France (e-mail: maxime.soma@inrae.fr).

Cédric Vega is with the ENSG, IGN, Laboratoire d'inventaire forestier, F-54042 Nancy, France (e-mail: cedric.vega@ign.fr).

Digital Object Identifier 10.1109/JSTARS.2023.3298991

geolocation errors in GEDI coordinates in slope terrain can result in larger elevation differences between the actual and provided coordinates than in flat terrain, it is reasonable to hypothesize that slope terrains will be more impacted by geolocation errors than flat ones.

Improving the georeferencing is important and requires specific approaches. The most widespread geolocation improvement method uses ALS data to simulate GEDI-like waveforms around the original footprint location [12], [22], [23]. The method processes by successive footprint clusters along individual ground tracks and a corrected geolocation is assigned where correlation between simulated and actual GEDI waveforms is maximized [12], [23]. Different studies used this approach to improve either v1 [12], [24] or v2 [17] data. Lang et al. [12] compared GEDI derived canopy heights with ALS heights, after geolocation correction, and obtained a 3.6 m root mean square error (RMSE) and a −0.3 m bias, while RMSE dropped to 2.7 m and bias to −0.1 m for 70% most certain position predictions, i.e., highest correlations between real and simulated waveforms. Liu et al. [17] compared ground elevation accuracy for v2 with and without geolocation correction and observed that improving geolocation led to a slight decrease in RMSE and in mean absolute error (MAE) of 0.12 m (4.15 m without and 4.03 m with correction) and 0.33 m (2.13 m without and 1.80 m with correction), respectively. Furthermore, Ni et al. [25] provided a comparison for AGB models based on relative height (RH) metrics obtained from v1 and v2, and from an optimized geolocation based on waveform matching of v1. When geolocation of v1 data was optimized, the determination coefficient (R^2) of the RH-based AGB model was sharply improved compared to v1 and slightly better than the one obtained with v2 data.

The method presented in Hancock et al. [23] has been primarily and successfully used to improve GEDI georeferencing. However, it requires waveform simulation from ALS data and is therefore limited to areas surveyed with ALS system, ideally at a time close to GEDI acquisitions. The method also requires downloading GEDI waveforms, a level 1 (L1) product that needs significant storage capacity and is not as user-friendly as higher level products. To overcome these limitations, the aim of this article is to develop an alternative georeferencing method based on the hypothesis that ground elevation data from reference digital elevation model (DEM) and GEDI level 2 (L2) ground elevation estimates are sufficient to improve the geolocation of GEDI footprints and to assess its performance. The approach, henceforth, referred to as GeoGEDI, should benefit from high-resolution DEM increasing availability and temporal stability, thus enabling much broader use. GeoGEDI was tested on v1 and v2 data for different forest and terrain conditions. Its performance was evaluated by analyzing magnitude and direction of the corrections and the impact on GEDI ground elevation and canopy height errors. The rest of the article is organized as follows. Section II introduces the data used to test and evaluate GeoGEDI. In Section III (method), GeoGEDI algorithm is detailed, prior to the presentation of the experimental setup and statistical analyses. Results are reported and discussed in Sections IV and V, respectively. Finally, Section VI concludes this article.

II. Data

A. Study Sites

Two contrasting French forest environments were considered, the Landes de Gascognes, or Landes' lowland forest, and the Vosges mountainous area. The Landes region is located in southwestern France and cover the largest metropolitan French forest. The relief of the Landes is mainly flat, with elevations ranging from 0 to 200 m and mean slope of 2.6% (±4.7%). Forests account for 74% of the area and are almost entirely composed of maritime pine (Pinus pinaster Ait) plantations [26], with an average canopy cover of 45% (±23%), measured at plot level by the National Forest Inventory. The Vosges site is located in northeastern France and is much more heterogeneous in terms of topography and forest stands. It covers part of the Vosges forest and the Haguenau forest, a large lowland forest. Elevations range from 100 to 1200 m, with mean terrain slope of 17.8% (±17.0%). Dominant species are European beech (Fagus sylvatica), silver fir (Abies alba), and Norway spruce (Picea abies) [26]. The forest cover is dense with mean canopy cover of 78% (±21%). Study sites were bounded by the extents of reference digital height models (DHMs) (see Section II-C-1). The Landes study site covers 14 051 km^2 and the Vosges study site covers 6 264 km^2. They will further be referred to as Landes and Vosges.

B. GEDI L2A Data

The GEDI instrument is composed of three lasers emitting 14 ns long near-infrared laser pulses at high frequency (242 Hz). One laser is split into two coverage beams, while the other two lasers produce two full-power beams. Each beam is deflected every other shot by the beam dithering units, which results in eight parallel ground tracks. Tracks are spaced 600 m apart and composed of 25 m diameter circular footprints 60 m apart along-track. For each footprint, the lidar waveform backscattered by the Earth's surface is recorded [2]. The recorded waveforms are processed to provide GEDI data products at footprint level. In GEDI L2A products, ground elevation, top of canopy, and RH metrics are derived from geolocated waveforms (L1B product). RHs correspond to cumulative waveform energy from bottom (0%) to top (100%), in 1% increments (RH0 to RH100) [27].

GEDI L2A products over study sites were downloaded from NASA's archive center [28], [29]. A total of 30 and 15 orbits crossing Vosges and Landes sites, respectively, and for which both version 1 (v1) and 2 (v2) GEDI products are available, were selected. Acquisition dates range from May 2019 to May 2020. The latitude, longitude, and elevation of the lowest mode (i.e., ground peak) were assimilated to footprint center coordinates and mean ground elevation within the area covered by the footprint, respectively. RH98 was used to assess the maximum height as suggested in [11] and [22]. To avoid issues with poor quality data in forest environment, only full-power footprints with good quality flags were used, as recommended in [11]. After filtering, Landes and Vosges study sites were sampled with 73 280 and 78 719 footprints, respectively (total: 151 999 footprints, Fig. 1).

TABLE I
DATA AND SOURCES

Data	Coordinate system	Source	Processing
GEDI L2A footprints version 1 and version 2	WGS 84	NASA [28],[29]	Filtered on full-power beams, quality flag, and availability of version 1 and version 2 Transformation to fit Lambert-93 coordinate system
Vosges DEMref	Lambert-93	IGN [30]	25-m focal mean of aerial lidar DEM
Landes DEMref	Lambert-93	IGN [30]	25-m focal mean of aerial lidar DEM
Vosges DHMref	Lambert-93	IGN	25-m focal maximum of aerial lidar DHM
Landes DHMref	Lambert-93	IGN	25-m focal maximum of photogrammetric DHM
BD Forêt v2	Lambert-93	IGN [32]	

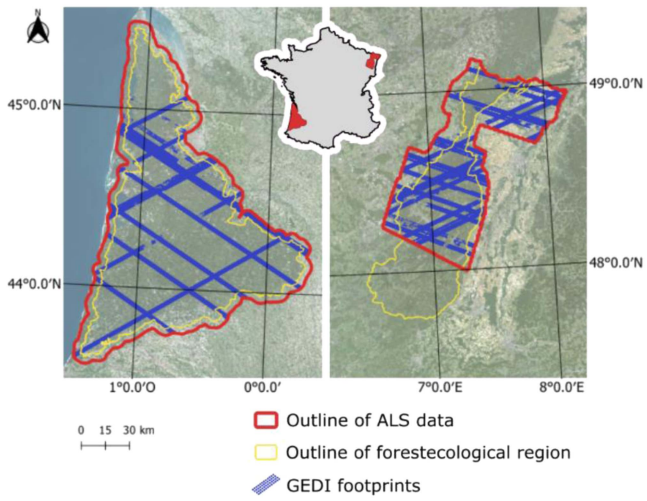

Fig. 1. Overview of GEDI footprints (in blue) in the two study sites (in red): Landes (left) and Vosges (right). The Landes de Gascognes and Vosges mountains forest's official ecological border are represented in yellow.

C. Reference Datasets

1) High-Resolution DEM and DSM: DEMs at a spatial resolution of 1 m were downloaded from the BD ALTI product of the National Institute of Geographic and Forest Information (IGN) [30]. For both study sites, the DEMs were derived from ALS acquisitions and delivered with altimetric and planimetric mean quadratic errors within 0.2 and 0.6 m, respectively [31]. Digital surface models (DSMs) representing the top of canopy, top of buildings, or other first return objects were also acquired from IGN, at the same spatial resolution. They were generated from either photogrammetric or ALS point clouds. DSMs were chosen in order to have a minimal temporal acquisition difference with GEDI data. For the Landes, the chosen DSM was produced using a photogrammetric point cloud generated using aerial photographs acquired in summer 2018 at a 35-cm resolution and processed using MicMac dense matching algorithm [32]. For the Vosges, the DSM was computed using ALS data acquired in winter 2020, and characterized by an average first return point density of 4.8 pt/m^2. On both sites, a DHM was obtained by subtracting ALS DEM from DSM. To allow for comparison with GEDI products, DEMref and DHMref, a 1-m resolution focal mean DEM and focal maximum DHM, were computed by using a sliding 25-m diameter circular window at each pixel.

2) Forest Database: BD Forêt v2 [33] provides information about the composition and density for forest stands which have areas of greater than 5000 m^2. The open-source database was used to classify footprints as forest or nonforest.

The different datasets are summarized in Table I.

III. METHOD

In this section, the GeoGEDI method is presented (in Section III-A) and the experimental setup is designed (in Section III-B). The latter includes parameter settings and filtering criteria used before analyzing algorithm outputs. The statistical analyses used to assess the algorithm performance are presented in Section III-C. The official French coordinate system, Lambert 93, was used during all the processing steps and analyses. While all IGN datasets were given in Lambert 93, GEDI data had to be transformed from WGS84 to Lambert 93. GEDI's latitude and longitude coordinates were transformed to Lambert 93 coordinates and GEDI's ellipsoidal heights were transformed to fit Lambert-93 altitude system by applying an altimetric conversion grid [34].

A. GeoGEDI Algorithm

GeoGEDI aims to match GEDI ground elevations to a reference DEM. Therefore, two inputs are needed: 1) GEDI footprint positions and ground elevations, and 2) DEMref. Each footprint F_i (with i ranging from 1 to the total number of footprints in the study area) is processed independently. However, coregistration relies on footprints clusters (Fig. 2). For each footprint F_i, the cluster C_i is made of n_i footprints acquired in a short time interval (δ_{time}) centered on F_i acquisition time. ISS structural vibration frequency is estimated between 0.1 and 1 Hz [35], [36], which is lower than the GEDI laser emission frequency (242 Hz). Consequently, it can be assumed that position errors of footprints belonging to a small cluster C_i are temporally correlated. During the small amount of time considered for a cluster, the pointing deviations due to ISS movements and vibrations will be similar in direction and magnitude. The lasers will not be randomly pointing in different directions and the cluster mean shift can be used to correct the position of Fi. C_i's optimal position (Δ_{opt}) is searched within a maximal distance of $\pm\text{shift}_{\max}$ (m) in X and Y and with a shift step (δ_{shift}) defined as a multiple of the DEMref resolution [i.e., k*r, with k $\in \mathbb{N}^*$ and r, the resolution of DEMref (i.e., 1 m here)]. This results in

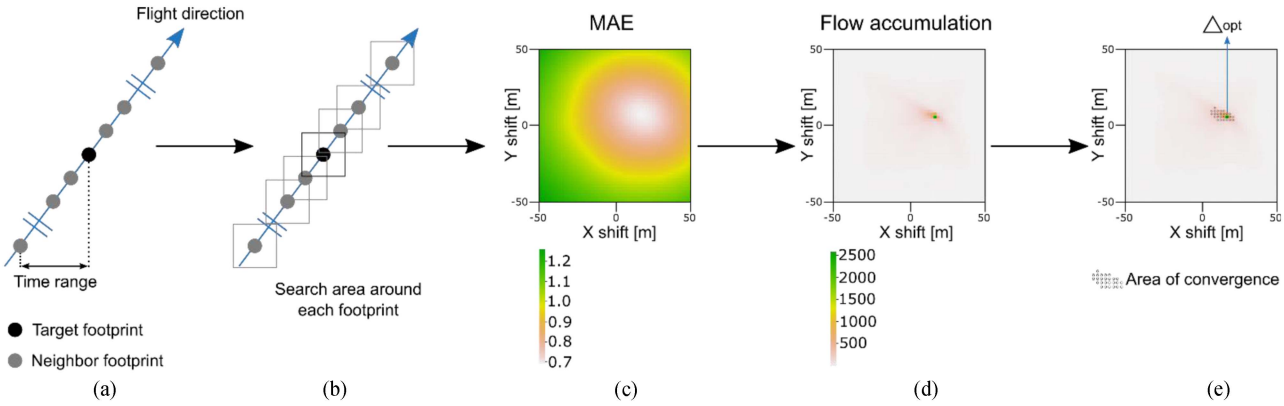

Fig. 2. (a) and (b) processing of a given footprint with its neighborhood. (c) Computation of mean absolute error map (MAE). (d) Error flow accumulation. (e) Computation of the optimal position from filtered accumulations barycenter.

a ($2^*\text{shift}_{\max}+1$) wide squared area for the search and in a set of $N_{\text{shift}} = ((2^*\text{shift}_{\max}/\delta_{\text{shift}})+1)^2$ positions tested for each footprint. The values selected for $\text{shift}_{\max}$ and δ_{shift} are presented in Section III-B-1 focusing on GeoGEDI parametrization. At each tested position, the MAE [MAE_p (1)] between C_i footprint elevations and the underlying DEMref elevations is computed as follows:

$$\text{MAE}_p = \frac{1}{n_i}\sum_{p=1}^{n_i}|z_p - \hat{z}_p| = \frac{1}{n_i}\sum_{p=1}^{n_i}|dz_p| \quad (1)$$

where

n_i number of footprints in the cluster;
z_p DEMref values;
$\hat{z}_p$ GEDI ground elevations; and
dz_p difference between z_p and $\hat{z}_p$.

Each MAE_p value is associated to its specific shift in X and Y from the initial footprint position, resulting in a 2-D MAE_i map providing a description of spatial error distribution according to shifts [Fig. 2(c)]. The best shift Δ_{opt} is computed from the MAE_i map using a two-step procedure. First, a divergent flow accumulation algorithm is applied to the MAE_i map [Fig. 2(d)]. The FD8 flow accumulation algorithm [37] was used (whitebox R package [38], [39])—a multidirectional flow algorithm commonly used to identify catchment areas and analyze drainage patterns in hydrological studies from raster DEMs. Unlike unidirectional algorithms, multidirectional flow algorithms allow flow dispersion and suit better in flat areas, while results between both types of algorithms are similar in the presence of slope [40], [41]. From each DEM cell, the flow is distributed toward the downslope neighboring cells according to proportions depending on the difference in elevation between the starting cell and its neighboring cells, i.e., the higher the difference, the higher the proportion [40], [41], [42]. The computation continues across grid cells until no more neighboring lower cell is encountered, i.e., once the flow has reached its catchment area. The final highest scores identify cells where flows most often stopped. When applied to the MAE_i map, flow accumulation leads to the point with the lowest error. Cells with highest scores highlight the areas corresponding to the shifts minimizing differences between DEMref and GEDI ground elevations. Second step: computing Δ_{opt} from the flow accumulation map. First, a convergence area is defined by selecting a given percentage of cells having the highest accumulation flow values. Then, Δ_{opt} is defined as selected cells' barycenter and computed as the average coordinates weighted by flow accumulation values. The approach integrates information from the entire error map and is relevant to address situations with no clear identified minima, for example, when several cells exhibited the same or similar maximum scores.

B. Experimental Setup

1) GeoGEDI Algorithm's Parameter Settings: Considering the positional accuracy of GEDI v1 provided in Beck et al. [7], we used 50 m as a reasonable upper shift limit ($\text{shift}_{\max}$). Even though the DEMref spatial resolution was 1 m, δ_{shift} was set to 2 m for computational efficiency. This results in $N_{\text{shift}} = 2601$ tested positions for each footprint. The convergence area was defined as the 1% cells having the highest accumulation flow value. This choice resulted from an experimental tradeoff to include enough pixels to describe the convergence area while limiting the selection of secondary convergence areas pixels.

GEDI laser units are fixed at different positions, with slight orientation differences, and each has its own depointing capacity, resulting in different viewing angles. Consequently, GeoGEDI should theoretically be applied to a cluster of footprints belonging to the same beam track, thus aligned on the ground. However, matching elevations along a single direction could be suboptimal for a robust footprint position adjustment. To overcome this limitation, GeoGEDI can be applied to a cluster including several beam tracks. To analyze the pros and cons of giving priority to the logic of acquisition geometry or 2-D spatial distribution of points when coregistering GEDI data and DEMref, GeoGEDI was applied by track or considering the four full-power beam tracks together, using the same time interval (δ_{time}). Selecting δ_{time} lower than the period of structural vibration of the ISS (0.1 to 1 Hz) is recommended. After testing several time intervals, δ_{time} was set to ± 0.215 s to select a sufficient number of footprints

for the adjustment, while avoiding large changes in shifts inside the cluster. This δ_{time} corresponds to a 3-km distance along a track and to ∼50 and ∼200 footprints for the single-beam and four-beam approach, respectively.

GeoGEDI was initially designed for GEDI v1 release. It was also applied to v2 data to demonstrate its potential for later releases with an improved geolocation. We hypothesize that the algorithm will also improve the later version, as NASA v2 products are said to be corrected for biases only, while GeoGEDI is supposed to improve the precision, i.e., to correct for nonsystematic errors due to ISS vibrations, in addition to correcting biases. For each of the 151 999 footprints, GeoGEDI was applied with four configurations. The different GeoGEDI outputs based on v1 or v2, using either the single-beam or four-beam approach, will be referred to as v1_1, v1_4, v2_1, and v2_4.

2) Data Filtering: Once the shifts were computed, several filters were applied. First, footprints associated to too small clusters were discarded. Indeed, cluster size (n_i) can be lowered due to removing low-quality footprints (see Section II-B). Threshold value was set to 1/4 of the theoretical maximum number of footprints for the considered time interval, corresponding to 13 and 50 footprints for the single-beam and four-beam approaches, respectively. All footprints that did not meet one of the abovementioned criteria, with either v1 or v2 dataset, were excluded. From the 151 999 footprints, 150 093 were kept for further analysis. Second, in each data set, i.e., v1_1, v1_4, v2_1, or v2_4, footprints where the shift in X or Y for Δ_{opt} reached $\text{shift}_{\max}$ (i.e., 50 m) were discarded.

Finally, some footprints were discarded due to issues identified in GEDI ground elevation assessment. Six waveform interpretation algorithms (01 to 06) were defined by the GEDI science team to identify the ground peak from GEDI waveforms, with different thresholds and smoothing settings [7], [27]. In GEDI L2A data v1, the default algorithm for all footprints was algorithm 01. In v2, the presumed best ground elevation is provided for each footprint along with the corresponding algorithm. This leads to possible changes in best algorithm choice and in differences in ground detection and elevation between the two GEDI versions. For v1, the default choice is always algorithm 01. For v2, the selected optimal algorithm was either 01 or 02 for our study sites. A comparison with DEMref revealed great ground elevation underestimation for some footprints where algorithm 02 was selected, probably due to faulty ground peak detection (Fig. 3 and Appendix A, Table V). To eliminate these misestimations in further analyses, footprints having a ground elevation difference between v1 and v2 of more than 1.5 m were discarded. This concerned 26.9% and 39.3% of footprints processed with algorithm 02, corresponding to 3.4% and 13.8% of footprints, for Landes and Vosges, respectively.

Please note: this source of error was identified after processing footprints; and the footprints were used during the georeferencing process. To limit influence of erroneous ground peak detection when comparing error estimates for different datasets, they were discarded regarding ground elevation and surface height estimation analyses.

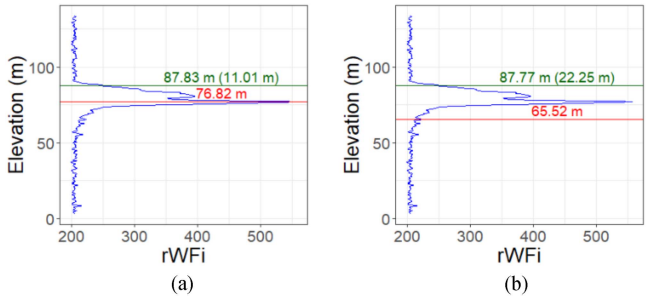

Fig. 3. Example of a sorted-out GEDI footprint waveform of (a) v1 using Algorithm 01 and (b) v2 using Algorithm 02. Ground elevation of the variable "lowest_mode" in red and RH98 transformed to surface elevation (and RH98) in green.

C. Statistical Analysis

Analyses were performed on the four GeoGEDI sets, i.e., v1_1, v1_4, v2_1, and v2_4. Statistics regarding differences between NASA v1 and v2, further referred to as v1_v2 results, were also reported as baseline for discussion. As effective GEDI footprint positions are unknown, GeoGEDI's performance can only be evaluated indirectly: 1) shifts were analyzed and 2) ground elevation and surface height errors were compared before and after applying GeoGEDI.

1) GeoGEDI's Shift Analysis: As GeoGEDI is supposed to correct for geolocation errors, checking whether GeoGEDI positions tend to be in the same direction and shifts of the same magnitude than NASA's is a complementary source of algorithm assessment.

Both shift magnitudes and directions were analyzed. In order to analyze mean shift directions while taking into account major differences in orientation between ascending and descending orbits as well as minor differences according to ISS's exact flight path, the coordinate system was changed. X and Y shifts, expressed according to West/East and South/North directions, were transformed into X_T and Y_T considering a coordinate system linked to the local orbit ground track direction. X_T axis follows the orientation of the orbit ground track [i.e., flight path direction relative to the West/East direction assessed by calculating the orientation of the track between the first and last footprint (of a same beam) of each orbit from v2 dataset] and Y_T axis is perpendicular to X_T, forming a local orthonormal coordinate system, centered on the initial footprint position (v1 or v2). Angular deviations can therefore be estimated when transforming new X_T and Y_T to polar coordinates, i.e., the footprints Euclidean distance to the initial position (0;0) and the shift angle relative to the track direction (X_T).

First, shift magnitudes' mean, median, and standard deviations were assessed. Then, mean relative shift distances and directions were used for dataset mean positions intercomparison. The mean positions were also compared by beam, so as to identify possible beam-dependent behavior.

Additionally, the temporal evolution of shift distances and directions was visually analyzed by plotting the positions of successive footprints belonging to the same orbit. For visual simplification, the temporal variability was illustrated for three

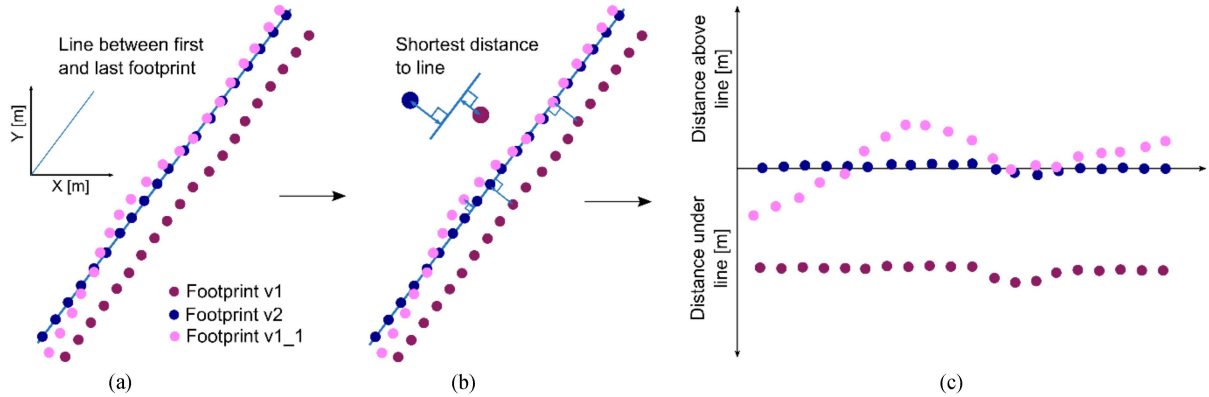

Fig. 4. (a) Illustrating the ground tracks of GEDI footprints and defining a reference track line. (b) Calculating each footprint's distance to the reference track line. (c) Plotting these distances.

datasets (v1, v2, and v1_1). It was assumed that orbit segments over the study areas can be assimilated to a line, and compared footprint position spread along that line for different datasets. To define the reference track line [Fig. 4(a)], we used the first and last v2 footprint of each track. Footprint Euclidean distances to the line were calculated [Fig. 4(b)] and reported on the final figure [Fig. 4(c)]. This highlights differences between ground tracks among the different datasets.

2) Elevations and Heights Qualification: GeoGEDI outputs are expected to improve the agreement between GEDI and reference elevations and heights. Therefore, ground elevation and surface height errors were analyzed. Ground elevation errors are expected to diminish as the algorithm is based on minimizing ground elevation errors. However, height errors analysis provides a fully independent evaluation of the algorithm performance. It consists in comparing GEDI RH98 data with DHMref.

The evaluation relied on four standard metrics: MAE (2), mean error [ME (3)], error standard deviation [σ (4)], and RMSE (5). These metrics were computed for the six different datasets (v1, v2, v1_1, v1_4, v2_1, and v2_4)

$$\text{MAE} = \frac{1}{n}\sum_{i=1}^{n}|z_i - \hat{z}_i| = \frac{1}{n}\sum_{i=1}^{n}|dz_i| \tag{2}$$

$$\text{ME} = \frac{1}{n}\sum_{i=1}^{n}(z_i - \hat{z}_i) = \frac{1}{n}\sum_{i=1}^{n} dz_i \tag{3}$$

$$\sigma = \sqrt{\frac{\sum_{i=1}^{n}\left(dz_i - \overline{dz}\right)^2}{n-1}} \tag{4}$$

$$\text{RMSE} = \sqrt{\frac{1}{n}\sum_{i=1}^{n}(z_i - \hat{z}_i)^2} = \sqrt{\frac{1}{n}\sum_{i=1}^{n} dz_i^2} = \sqrt{\text{ME}^2 + \sigma^2} \tag{5}$$

where

n	number of footprints in the dataset;
z_i	DEMref values;
$\hat{z}_i$	GEDI ground elevations;
dz_i	difference between $z_i$and $\hat{z}_i$; and
$\overline{dz}$	sample's mean difference between $z_i$and $\hat{z}_i$.

The same statistics were used for height estimations, replacing DEMref by DHMref and z by h.

For each footprint, available auxiliary information included: 1) the study site, 2) forest vs. nonforest status, 3) shift magnitude, 4) and a local slope indicator. The latter was defined as the ground elevation range at each GEDI footprint level, and was computed from the 1-m raster DEM using v1 footprint positions. Forest vs. nonforest status was established using both the forest map (see Section II-C-2) and DHMref. All nonforest footprints of the forest map were assigned the "nonforest" class, while forest footprints with a less than 2-m DHMref value were reclassified as "nonforest," in order to remove footprints acquired over clear-cuts or areas that changed from forest to agricultural land between the last forest map update and GEDI data acquisitions. Distributional metrics were compared for several datasets, defined based on auxiliary information. To evaluate the shift magnitude influence, footprints were divided into five classes based on quantiles of shift magnitude distribution, resulting in an equal number of footprints per classes. Classes were noted C_{Q1}, C_{Q2}, C_{Q3}, C_{Q4}, and C_{Q5}.

IV. Results

A. Shift Magnitudes and Directions

Table II shows GeoGEDI shift statistics for the different approaches. For GEDI v1-based approaches, mean shift values were similar across sites and ranged from 23.55 m (v1_1 Vosges) to 23.95 m (v1_4 Landes). Standard deviations proved higher for the Landes, ranging from 9.32 m (v1_4 Vosges) to 14.70 m (v1_1 Landes). As expected, shifts were of lower magnitude for v2-based than for v1-based approaches. For Vosges, mean values were divided by more than two while standard deviations were more stable [10.85 m ($\pm$8.61 m) and 11.84 m ($\pm$9.45 m) for v2_4 and v2_1, respectively]. For Landes, the shift magnitudes reduction was reflected by a decrease in medians by at least 4 m rather than by changes in mean and standard deviation underlying the possible presence of outliers in shift distributions. Moreover, mean shifts between v1 and v2 obtained by NASA

TABLE II
MEAN, MEDIAN (MED), AND STANDARD DEVIATION (σ) OF DIFFERENCES BETWEEN GEOGEDI AND CORRESPONDING NASA COORDINATES

	Landes			Vosges		
	Mean	**Med**	**σ**	**Mean**	**Med**	**σ**
v1_1	23.88	20.59	14.70	23.55	22.80	10.07
v1_4	23.95	21.63	13.46	23.64	23.32	9.32
v2_1	22.19	16.12	16.62	11.84	8.94	9.45
v2_4	20.48	14.42	16.72	10.85	8.25	8.61
v1_v2	17.80	17.18	4.52	20.60	20.51	3.88

The last line corresponds to distances between v1 and v2. Units are given in m.

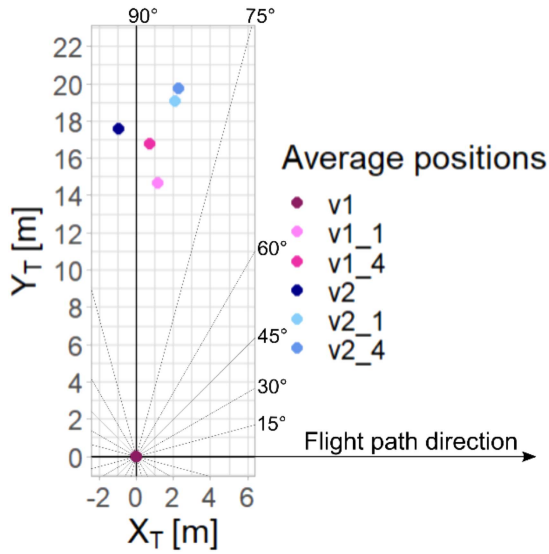

Fig. 5. Average relative positions between the different approaches (including both study sites). The flight path direction is used as *X*-axis and GEDI v1 is used as coordinate axis origin.

(v1_v2) were 17.80 m (±4.52 m) for Landes and 20.60 m (±3.88 m) for Vosges.

Fig. 5 illustrates the relative average positions in X_T and Y_T between the different datasets. As a visual convention, the position of v1 was used as the coordinate system's origin (0;0). In average, all corrections led to positions characterized by both a similar direction (83° to 93°) and magnitude (14.69 to 19.83 m). The NASA correction led to an average position at a distance of 17.59 m from v1 position and in a direction of 93.00° with respect to v1 track direction. Average positions obtained using GeoGEDI on v1 showed distances of 14.69 and 16.79 m in directions of 85.31° and 87.33° for v1_1 and v1_4, respectively. Average GeoGEDI corrected positions v2_1 and v2_4 are very close to each other, with 19.17 and 19.84 m at 83.63° and 83.33°, respectively, from v1 positions. If only Vosges footprints are taken into account, all four GeoGEDI average positions, i.e., v1_1, v1_4, v2_1, and v2_4, are grouped within 19.19 and 22.88 m distances and 86.78° and 87.95° directions.

Although footprints average corrected positions were relatively close to each other, there were notable differences among experimental setups. Fig. 6 illustrates the spread in shift distributions for an example orbit. Fig. 6, unlike Figs. 5 and 7, is presenting the applied shifts in *X* and *Y* coordinate system, i.e., following the usual West/East and South/North axis, in order to illustrate the shifts with regards to the search window. NASA's shifts (i.e., v1_v2) are concentrated around the mean value with a 18.37 m maximum shift and mean and standard deviation shift magnitude of 13.69 m (±1.59 m). Shifts are more spread for v1_1 and v1_4 with means (±σ) of 22.96 m (±9.45 m) and 25.1 m (±6.39 m), respectively. The global trend in shift corresponds to the bias correction, while the dispersion in shifts around this trend corresponds to the correction of the non-systematic error component and results in an increase in precision.

GeoGEDI average positions according to beam configurations are provided in Fig. 7. Mean shifts perpendicular to the flight axis were quite similar whatever the beam and approach, while shifts parallel to the flight path showed greater variations according to the beam and emitting laser. Beams acquired by the same laser, i.e., beams 0101 and 0110, and beams 1000 and 1011, respectively, exhibit similar shifts. For v1_v2, intrabeam pair distances were 1.29 and 2.83 m for beam pairs (0101, 0110) and (1000, 1011), respectively, and mean distances between the two beam pairs ranged between 7.86 and 11.81 m. Beams 0101 and 0110 were rotated by 107.02° and 111.14° from v1 track direction, while beams 1000 and 1011 were rotated by 74.60° and 81.63°. Similar results were obtained for v1_1, with intrabeam pair 0.80 and 0.46 m distances, respectively, and interbeam pair distances from 5.49 to 6.21 m. The angles obtained by beam pairs were very close to each other with 96.24° and 97.10° for the first pair, opposed to 76.06° and 76.36° for the second pair. As expected, mean shifts were grouped together using the four-beam approach [Fig. 7(c)] with mean positions being 0.07 to 0.28 m apart. The beam pairs are no longer standing out for v2_1 [Fig. 7(d)]. For v2_1, intrabeam pair distances were 0.30 and 0.70 m and interbeam pair distances ranged between 0.38 and 0.66 m. Rotation angles were between 20.39° and 30.46°. For v2_4, average positions are also grouped together, with interbeam distances ranging from 0.04 to 0.36 m at a maximum distance of 4.00 m from the original v2 position and angles ranging from 31.87° to 34.74°.

Fig. 8 illustrates GeoGEDI positions' temporal evolution for an orbit segment and highlights differences between ground tracks corresponding to the various datasets. V1 and v2 tracks are nearly parallel, which translates the bias correction announced by NASA. Tracks obtained with GeoGEDI wobble around v2 tracks, and may vary quickly over time, as illustrated in Fig. 8. In Landes, local variations are greater than in Vosges. Within only 3 km, the v1_1 track can deviate by more than 50 m from the reference track line [Fig. 8(c)].

B. Impact of GeoGEDI Corrections on Ground Elevation and Surface Height Estimates

Next, the differences between DEMref and GEDI ground elevations and between DHMref and GEDI RH98 are referred to as *dz* ($Z_{\mathrm{DEMref}} - Z_{\mathrm{GEDI}}$) and *dh* ($H_{\mathrm{DHMref}} - H_{\mathrm{GEDI}}$), respectively.

1) Evaluation of Ground Elevation and Surface Height for Forest and Nonforest Areas: Table III shows ground

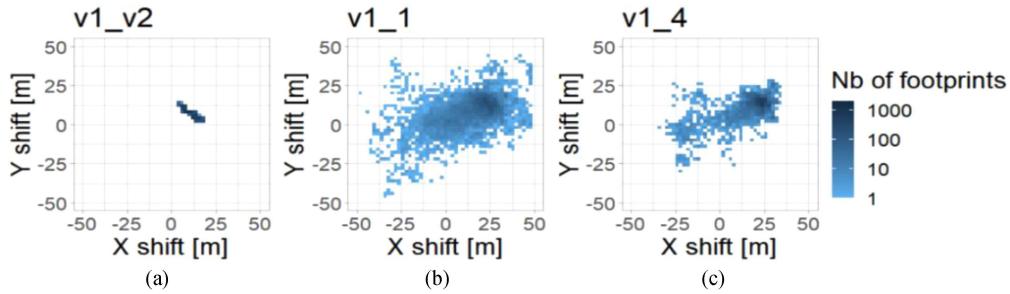

Fig. 6. All individual shifts applied to footprints from orbit 3144 intersecting Landes. (a) v2 compared to v1. (b) Single-beam approach on v1. (c) Four-beam approach on v1. The original latitude-/longitude-oriented coordinate system is used for this illustration.

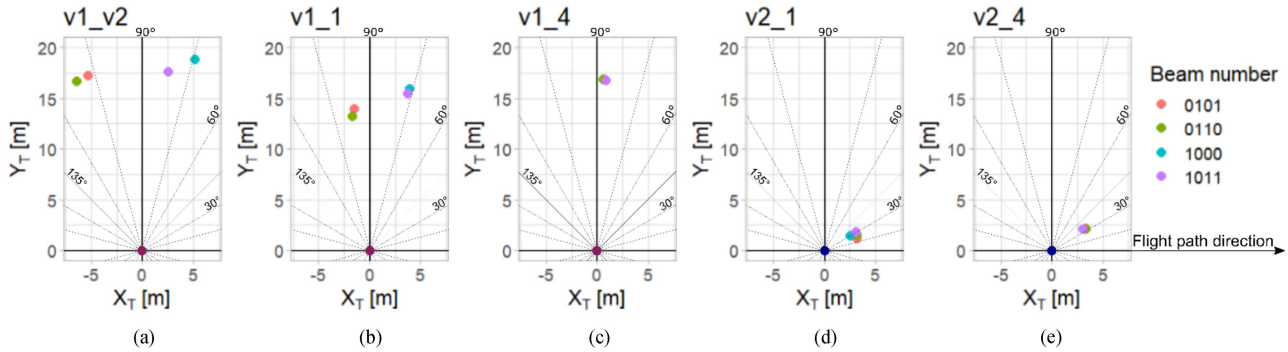

Fig. 7. Average relative positions by beam, for all footprints between GeoGEDI and corresponding NASA coordinates. (a) v2 compared to v1. (b) v1_1 compared to v1. (c) v1_4 compared to v1. (d) v2_1 compared to v2. (e) v2_4 compared to v2. The flight path direction is used as *X*-axis and GEDI v1 positions were used as coordinate axis origin for (a), (b), and (c) and GEDI v2 for (d) and (e).

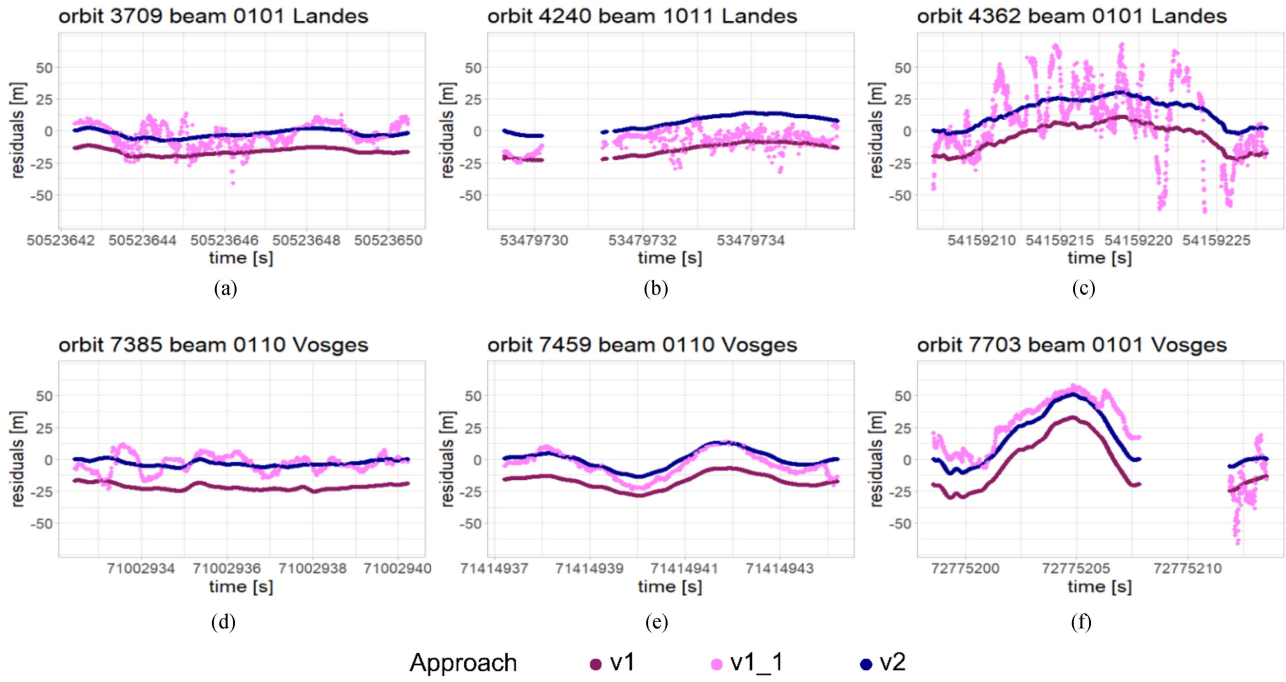

Fig. 8. Temporal variability of v1, v2, and v1_1 ground tracks for three orbits in Landes (a, b, c) and in Vosges (d, e, f). A reference track line was defined between first and last v2 footprints and plots show the distance of footprints to the reference line. Time corresponds to the delta_time variable of GEDI footprints.

TABLE III
GROUND ELEVATION ERRORS FOR ALL SIX DATASETS FOR FOREST AND NONFOREST FOOTPRINTS

	Landes						Vosges					
	Forest (n ≈ 43 900)			Non forest (n ≈ 24 000)			Forest (n ≈ 36 800)			Non forest (n ≈ 29 500)		
	ME	**σ**	**RMSE**	**ME**	**σ**	**RMSE**	**ME**	**σ**	**RMSE**	**ME**	**σ**	**RMSE**
v1	−0.36	1.22	1.27	−0.30	1.06	1.11	−0.36	6.40	6.41	−0.50	2.37	2.42
v1_1	**−0.28**	**0.89**	**0.93**	**−0.23**	**0.76**	**0.79**	**−0.20**	**2.58**	**2.59**	**−0.33**	**0.96**	**1.01**
v1_4	−0.30	0.91	0.96	−0.23	0.77	0.81	−0.33	2.86	2.87	−0.42	1.05	1.13
v2	−0.50	0.92	1.05	−0.46	0.77	0.90	−0.48	3.87	3.90	−0.63	1.26	1.40
v2_1	**−0.41**	**0.82**	**0.91**	**−0.37**	**0.69**	**0.78**	**−0.42**	**2.46**	**2.49**	**−0.46**	**0.87**	**0.98**
v2_4	−0.43	0.85	0.95	−0.38	0.69	0.79	−0.43	2.53	2.56	−0.54	0.88	1.04

Best results for v1- and v2-based approaches are highlighted in bold.

TABLE IV
SURFACE HEIGHT ERRORS FOR ALL SIX DATASETS FOR FOREST AND NONFOREST FOOTPRINTS

	Landes						Vosges					
	Forest (n ≈ 43 900)			Non forest (n ≈ 24 000)			Forest (n ≈ 36 800)			Non forest (n ≈ 29 500)		
	ME	**σ**	**RMSE**	**ME**	**σ**	**RMSE**	**ME**	**σ**	**RMSE**	**ME**	**σ**	**RMSE**
v1	0.76	5.19	5.25	−1.41	4.81	5.01	2.69	6.98	7.48	−1.10	7.50	7.58
v1_1	0.68	4.93	4.98	−1.34	4.49	4.68	2.44	5.65	6.16	−0.86	6.60	6.65
v1_4	**0.64**	**4.69**	**4.74**	**−1.28**	**4.28**	**4.47**	**2.43**	**5.59**	**6.09**	**−0.84**	**6.56**	**6.61**
v2	**0.54**	**4.45**	**4.48**	**−1.12**	**4.04**	**4.19**	2.41	5.82	6.30	−0.87	6.59	6.64
v2_1	0.69	4.94	4.99	−1.35	4.58	4.77	2.38	5.62	6.10	**−0.84**	6.55	6.60
v2_4	0.69	4.76	4.81	−1.29	4.37	4.55	**2.38**	**5.49**	**5.99**	−0.85	**6.44**	**6.50**

Best results for v1- and v2-based approaches are highlighted in bold.

elevation errors for study sites, by land use (i.e., forest and nonforest). Overall, GEDI overestimated ground elevations. The smallest (−0.2 m) and greatest (−0.63 m) overestimations were observed in the Vosges site, for v1_1 forest footprints and v2 nonforest footprints, respectively. For both land uses, both study sites and both GEDI versions, GeoGEDI outputs systematically decreased ground elevation errors compared to NASA's versions. For Vosges, RMSEs were decreased by 59.6% and 58.3% for v1 and by 36.2% and 30.0% for v2, for forest and nonforest footprints, respectively. For Landes, RMSEs were decreased by 26.8% and 28.8% for v1 and by 13.3% and 13.3% for v2, for forest and nonforest footprints, respectively. Best results were achieved with single-beam adjustment. The lowest RMSEs were achieved with v2_1, with 0.91 and 2.49 m for forest and 0.78 and 0.98 m for nonforest areas, for Landes and Vosges, respectively. Interestingly, the standard deviations were much smaller for Landes (0.69–1.22 m range) than for Vosges (0.87–6.40 m range).

Surface height results are presented in Table IV. Overall, GEDI heights were closer to reference heights at v2 positions than at v1: ME, σ, and RMSE all decreased. The greatest height assessment improvements were achieved with the four-beam approach, except for v2 in Landes; there, GeoGEDI brought no improvement. For Vosges, slightly better performances were observed with v2-based approaches than with v1-based ones. In both sites, mean heights were underestimated for forest footprints—ME ranging from 0.54 to 0.76 m for Landes and from 2.38 to 2.69 m for Vosges—and overestimated for nonforest footprints—ME ranging from −1.12 to −1.41 m for Landes and from −0.84 to −1.10 m for Vosges. RMSEs were similar for both land uses, with values ranging from 4.19 (v2, nonforest) to 5.25 m (v1, forest) and from 5.99 (v2_4, forest) to 7.58 m (v1, nonforest), for Landes and Vosges, respectively. Overall, in Vosges, RMSEs were lower for forest footprints than for nonforest footprints. Opposite results were observed in Landes.

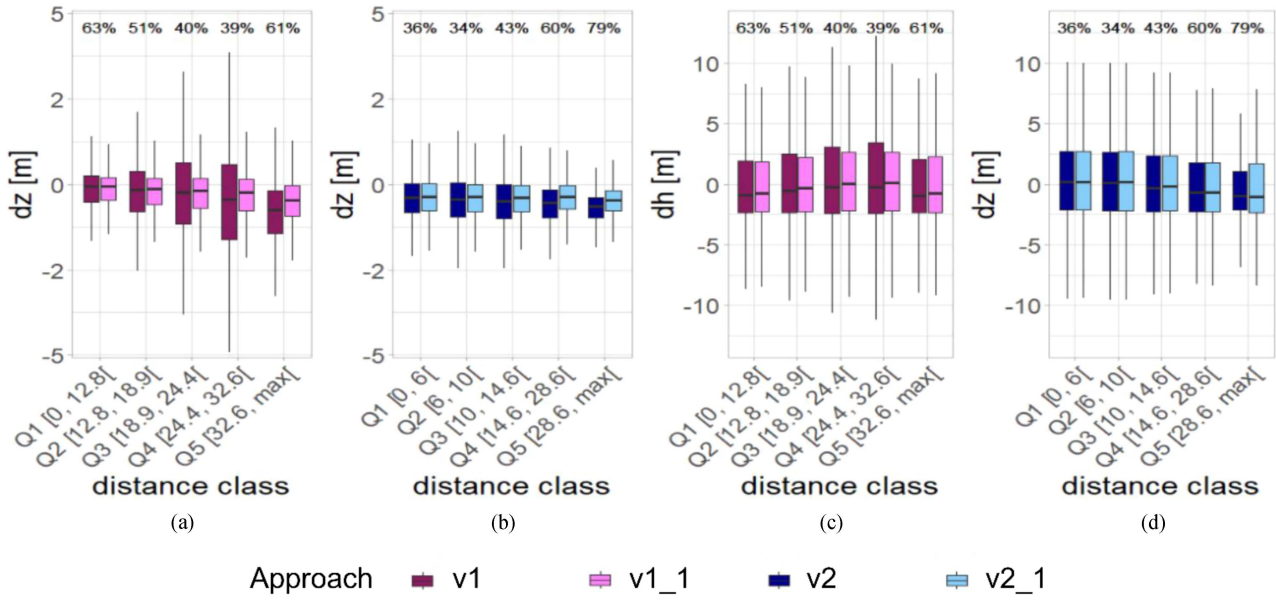

Fig. 9. (a), (b) Ground elevation errors (*dz*). (c), (d) Surface height errors (*dh*) for v1, v1_1, v2, and v2_1 approaches, by footprints shift magnitudes quantiles of v1_1 or v2_1 distances to the initial GEDI version (v1 or v2). Distances are given in meters, e.g., class *Q*1 for v1 includes all footprints which were moved by 0 to 12.8 m when applying v1_1 GeoGEDI algorithm. The percentage above each class indicates the part of footprints belonging to Landes study site. Remaining footprints belong to Vosges.

As both setups (single-beam and four-beam) gave similar results, only single-beam results are reported in Sections IV-B-2 and IV-B-3.

2) Shift Magnitudes Influence: GeoGEDI shift magnitudes impact on ground elevation and height estimates was considered, to evaluate whether large shifts were justified or artifacts. Fig. 9 compares *dz* distributions between v1 and v1_1 [Fig. 9(a)] and between v2 and v2_1 [Fig. 9(b)] for five shift magnitude classes (see Section III-C-2). The improvement in ground elevation accuracy increases with shift magnitude increase. For v1_1, RMSEs were lowered by 18.8%, 39.0%, 54.6%, 62.0%, and 68.1% for classes C_{Q1}, C_{Q2}, C_{Q3}, C_{Q4}, and C_{Q5}, respectively. The same trend, with a decrease in precision and an improvement in bias [Fig. 9(b)], was observed for v2, although improvements in accuracy were less pronounced. For v2, ground elevation RMSEs were, respectively, improved by 5.7%, 18.5%, 27.5%, 39.9%, and 61.0%. As already noticed, shifts applied to v2 were much smaller than those applied to v1 (see class limits, Fig. 9). For v1_1, 20% of footprints were shifted by less than 12.8 m, while for v2, this quantile limit was 6 m.

Regarding surface heights [Fig. 9(c) and (d)], compared to v1, v1_1 RMSEs decreased by 4.2%, 11.8%, 14.7%, 20.6%, and 6.4% for classes C_{Q1} to C_{Q5}. Like for ground elevations, the further the shift, the more important the improvement in height estimates in the first four classes. However, RMSEs did not continue to improve for C_{Q5}. Compared to v2, v2_1 height RMSEs were slightly improved by a maximum of 3.2% for the smallest shift distances (C_{Q1}, C_{Q2}, and C_{Q3}). But RMSE improved by only 0.6% for class C_{Q4}, and even deteriorated by 24%—from 4.55 to 5.64 m—for footprints belonging to C_{Q5} [Fig. 9(d)]. Note that C_{Q5} is mainly composed of Landes footprints (79% Landes against 21% Vosges).

3) Influence of the Slope: In sloped terrain, a small error in geolocation results in large ground elevation errors. As expected, the higher the slope indicator, the higher the errors in ground elevations [Fig. 10(a) and (b)]. For example, v1 ground elevation RMSEs were 0.98, 1.70, 2.87, 4.65, and 9.05 m for the five slope classes reported in Fig. 10. Moreover, the higher the slope indicator, the greater the improvement brought by GeoGEDI, and, compared to v1, v1_1 ground elevation RMSEs were improved by 9.7%, 31.3%, 48.2%, 59.2%, and 63.4%, for classes C_1, C_2, C_3, C_4, and C_5, respectively. Similar results were obtained for v2_1 regarding v2, with improvements of 5.7%, 12.7%, 21.4%, 31.7%, and 41.7% for all five slope classes.

The slope effect on height estimates is illustrated in Fig. 10(c) and (d). For all datasets, the smaller the slope, the better the estimate. For v1, GeoGEDI outputs improved the flattest footprints' height accuracy by 4.9%. For the other four classes, height RMSEs decreased between 18.1% and 20.8%. For v2_1, height RMSE increased by 9.6% for footprints with no slope (C_1) and height RMSE was improved by 1.7% for footprints with low slope (C_2). Concerning footprints with greater slope (C_3, C_4, C_5), height RMSEs were improved by 5.1%, 6.0%, and 5.7%, respectively.

V. Discussion

A. Shift Analyses Corroborate GeoGEDI's Efficiency

GeoGEDI-based mean shifts were in accordance with horizontal geolocation errors announced by NASA's user guide [7]. Logically, shifts obtained with v1-based approaches were greater than those obtained with v2-based approaches (Table II). Beck et al. [7] studied GEDI geolocation error over a 30-week time-span. The mean of weekly computed 1 σ errors was

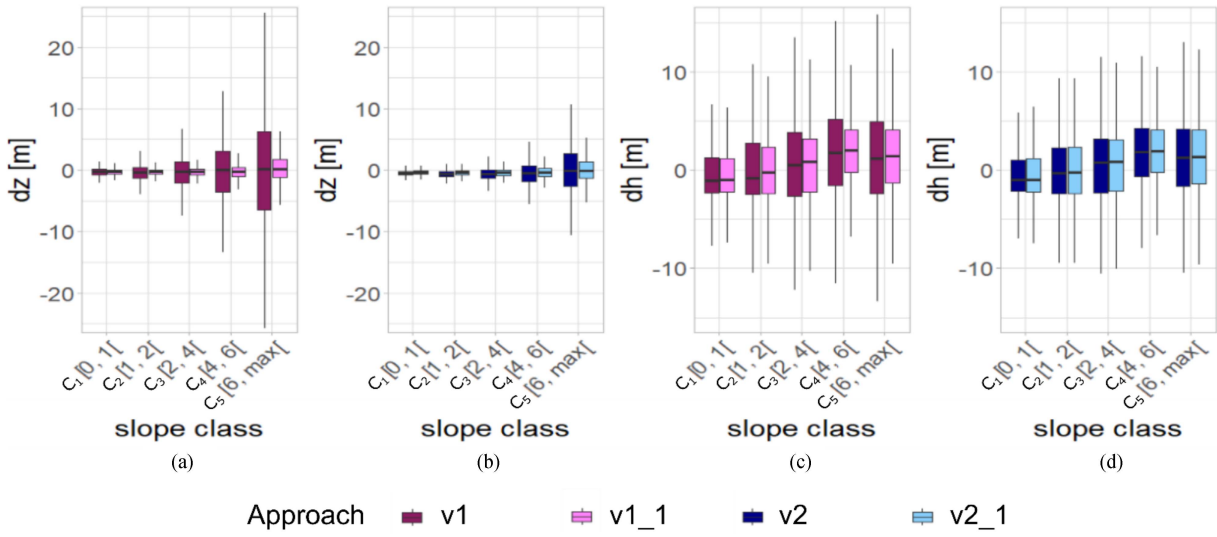

Fig. 10. (a), (b) Ground elevation errors (*dz*). (c), (d) Surface height errors (*dh*) for v1, v1_1, v2, and v2_1 approaches, by footprints slope indicator. The slope indicator corresponds to the elevation range in the 25 m circular footprint and is given in meters.

23.8 m with a substantial bias [4], and 10.2 m with a limited bias for v1 and v2, respectively. GeoGEDI's v1-based mean shift distances were within this range, with 23.55 to 23.95 m mean shifts. For v2-based approaches, GeoGEDI results varied among sites. Mean shifts for Vosges were close to the 10.2 m geolocation error announced by NASA, with values of 11.84 m (v2_1) and 10.85 m (v2_4). Mean shifts for Landes reached 22.2 and 20.5 m and were therefore close to the 2 σ mean error announced by NASA, challenging GeoGEDI outputs over large flat areas (see Section V-B). Nevertheless, all GeoGEDI positions converged toward v2 mean positions resulting from the in-flight NASA-operated calibration (Fig. 5), thus providing additional GeoGEDI robustness validation. The on v1 applied corrected angles all rotated toward the same direction, above and perpendicular to the flight path direction. Compared to initial v1 positions, v2 positions were moved in a direction of ∼93° with respect to v1 track direction and GeoGEDI v1_1 and v1_4 in a direction of ∼85° and ∼87°, respectively. This is in line with the direction found by Quirós et al. [21]. In order to correct the positions for geolocation bias, they tested eight directions (0°, 45°, 90°, 135°, 180°, 225°, 270°, and 315°) at two distances (5 and 10 m) from the initial v1 position and defined the best fitting position for each footprint based on the lowest RMSE between GEDI elevation and aerial lidar DEM. Among the 17 tested positions (e.g., eight directions at two distances and the central initial position), the best fitting position was at 10 m and 270° clockwise, corresponding to a 90° angle above the flight path (i.e., standard counterclockwise angle measurement used in this article). A total of 31.88% of their footprints had the lowest RMSE for this position.

Moreover, GeoGEDI per beam results complied with theoretical expectations. When the single-beam approach was applied to v1, resulting mean positions were paired according to laser units. Nevertheless, mean positions also exhibited small differences, possibly arising from the difference in pointing direction between the two beams of a beam pair emitted by the same laser unit. Compared to initial v1 positions, v2 positions were rotated by ∼78° for one beam pair and by ∼109° for the other pair. GeoGEDI v1_1 average positions were rotated by 76° for beam pairs 1000 and 1011, while beams 0101 and 0110 were rotated by ∼97°. When applied to v2, GeoGEDI mean shifts were almost identical for all beams regardless of the laser unit, confirming NASA's biases correction on v2 products. Mean positions of v2_1 and v2_4 corrected initial v2 positions with 20° to 35° angles.

Finally, we assumed GeoGEDI could correct for geolocation source inaccuracy that cannot be handled from ISS-borne sensors and in-flight calibrations, such as ISS structural vibrations. Beyond the trends provided by mean shifts, the quick shifts temporal changes and their magnitude are worth noticing. For both, the single-beam and the four-beam approaches, two consecutive footprints could have significantly different shifts with respective clusters differing by few footprints. Yet, shift values followed a relatively continuous pattern (Fig. 8). This continuity is important, as it is key for our assumption validity, i.e., using footprints acquired in a shorter time interval than the highest vibration period captures these vibrations impact on the geolocation error. Resulting GeoGEDI tracks have more variable and less "smoothed" track patterns than those observed in NASA footprint positions, highlighting that GeoGEDI succeeded in capturing part of ISS high frequency variations. As a result, computed shifts were observed as spatially correlated (shift continuity). However, we are aware that GeoGEDI tracks are probably still slightly smoothed compared to real tracks, as footprints were corrected for local mean deviations.

B. GeoGEDI Advantages and Limitations

The proposed georeferencing method proved efficient and robust for a diversity of environments (Section V-B-1), even if some limitations (Section V-B-2) and possible ways of improvements (Section V-B-3) were identified.

1) GeoGEDI Main Strengths: One of GeoGEDI's major assets is it needs only two inputs: 1) coordinates and "lowest_mode" variable from GEDI L2A footprints and 2) a high-resolution DEM, which are increasingly available worldwide. Additionally, it is simpler than methods based on waveform correlation between GEDI and ALS simulations [23]. Results indicated that GeoGEDI greatly improved consistency in ground elevation between GEDI and DEMref (see Section IV-B-1). Height estimates were also improved for most cases, except for v2-based approaches in Landes (see Section V-B-2). Consistency between GEDI estimations and reference values proved considerably improved in sloped areas where even small geolocation error can lead to high discrepancy.

Note that GeoGEDI results are in the same range as Hancocks' waveform matching approach. After correcting v1 for geolocation, Ilangakoon et al. [24] and Lang et al. [12] observed 4.69 and 3.6 m GEDI surface heights RMSE for their study sites, respectively, while v1-based GeoGEDI reached 4.47 to 6.65 m RMSEs. For ground elevations, after correcting v2, Liu et al. [17] observed a 4.03 m RMSE value, while GeoGEDIs range from 0.79 (nonforest, Landes) to 2.59 m (forest, Vosges). Relative improvement between v2 and corrected v2 can be computed from results in [17]. MAE was improved by 15.5% and RMSE by 2.9%, while GeoGEDI's v2 approaches improved RMSE ground estimations by minimum 13.3% (forest and nonforest, Landes) and up to 36.2% (forest, Vosges).

However, results on ground elevation and canopy height accuracy after improving the geolocation were still and inevitably influenced by study site characteristics. The Landes are flat and stands are mainly composed of maritime pine, a species that lets a high proportion of light reach the ground. On the contrary, in the topographically complex area of the Vosges mountains, stands are more dense and are composed of species with higher foliage density. Several studies have reported a link between an increase in RMSEs and an increase in either vegetation density [15], [17], [21] or terrain slope [1], [17] for both GEDI ground elevation and vegetation height products. For example, Liu et al. [17] reported high ground RMSEs (6–7 m) for dense and tall vegetation and a 2.88 m RMSE for areas with slope $<5°$ compared to 6.70 m for areas with slope $>30°$. Similarly, errors for v1 and v2 forest footprints are much higher in the Vosges than in the Landes, and remain higher in the Vosges even after geolocation has been improved, e.g., v2_1 ground elevation RMSEs are 0.91 and 2.49 m and canopy height RMSEs are 4.99 and 6.10 m, in Landes and Vosges, respectively.

Concerning canopy heights estimations, they are directly impacted by ground estimation accuracy [17] and thus by the abovementioned factors. Despite a large geolocation bias correction, improvements in RMSEs between v1 and v2 remain limited [i.e., 5.25 m down to 4.48 m (-17 %) over the Landes and 7.48 m down to 6.30 m (-19 %) over the Vosges]. This can be attributed to the relative stability of vegetation height at stand level as both study sites are mainly occupied by even-aged production forests. Even once shifted, a majority of footprints will be located in the same stand and have a similar canopy height value than at their initial location.

The uncertainty of reference data may also affect the discrepancy between GEDI and reference data. Most importantly, the time and seasonal differences between the two data acquisitions allow for changes in vegetation heights. The Landes have significant forest dynamics in pine plantations [43], drastically impacting canopy heights.

2) GeoGEDI Limitations in Flat Areas: Validation highlighted better GeoGEDI performances for Vosges than for Landes. Shift distances v2_1 and v2_4 for Landes were also higher than for Vosges, departing from horizontal geolocation errors announced by the user guide [7]. Additionally, mean shift distances barely decreased between approaches applied on v1 and on v2. The presence of large flat areas in Landes might explain such results. Typically, DEMref values in Landes optimal position search windows are highly similar, which impedes convergence toward minimal error and finding the optimal position. The error analysis by shift magnitude classes [Fig. 9(d)] highlights issues with footprints belonging to C_{Q5} (shift $\geq$ 32.6 m) for v1 and to C_{Q4} and C_{Q5} (shift $\geq$ 14.6 m) for v2. While all classes' ground elevation estimates improved, surface height estimations of footprints with the largest shifts worsened. These classes may include footprints for which GeoGEDI converged toward a suboptimal position. These geolocation errors have more impact on height accuracy than on ground elevation estimates due to the lower variability in elevation compared to surface height variability. It is worth noticing that those very large shifts mainly concern Landes footprints (61% of the footprints in C_{Q5} in v1 and 79% of C_{Q5} in v2 belong to Landes). In Section III-B-2, we also reported that a subset of footprints was removed prior to statistical analyses because the convergence process was interrupted at the search window limit. This mainly concerned Landes footprints, with up to 8.7% of footprints compared to 1% in Vosges, suggesting the algorithm had punctually some converging issues in flat areas. The important dispersion of GeoGEDI shifts [e.g., Fig. 8(c)] can be explained by ISS large movements and vibrations, or by convergence issues in flat and textureless areas.

3) Recommendations on the Use of GeoGEDI and Possible Improvements: On the one hand, using the single-beam approach better respects the lidar systems acquisition geometry. On the other hand, using the four-beam approach increases the number of footprints in the cluster and spatial dimension (from 1-D profile to 2-D sampling), which is likely to increase elevation variability within the cluster, especially in low-relief areas. For v1-based approaches, best estimates were observed with the single-beam approach. Therefore, it is more important to respect the acquisition geometry than to build on the beneficial effect of 2-D sampling. To improve georeferencing of v1 data, the single-beam approach should be preferred in all cases. Processing GeoGEDI by beam pair clusters could also be considered in future studies, increasing the number of footprints, while respecting the instrument geometry. NASA v2 geolocation was corrected for bias and is less, or even no more impacted by acquisition geometry effects thanks to in-flight calibration. Therefore, the four-beam approach can be considered on v2. Single-beam and four-beam approaches gave

very similar GeoGEDI outputs. GeoGEDI v2_1 estimates were slightly better for ground elevations, whereas v2_4 estimates were slightly better for surface height estimates. Both approaches can be used to further improve GEDI v2 geolocation. However, assessing height estimates aimed to provide an independent validation, suggesting that the four-beam approach should be preferred to process v2 data.

Furthermore, in low-relief environment, increasing the cluster size would increase heterogeneity in elevations, allowing better convergence of the flow accumulation algorithm. However, it would also result in "smoother" tracks closer to v2 tracks, and thus to lower improvement in geolocation precision with less consideration to errors due to high frequencies vibrations. Moreover, as it is only based on GEDI and DEMground elevations, GeoGEDI would certainly benefit from improved ground peak detection in L2A data. Indeed, even if GeoGEDI improved estimates, footprints with sharp local ground underestimates were included during adjustment process and might have impacted GeoGEDI's v2-based outputs.

Results could also be improved by increasing the search window beyond 50 m and by using a smaller shift step, e.g., equal to the DEMref resolution (1 m), instead of the 2-m δ_{shift} that was used in this article. However, this would result in a sharp computation time increase, and should be accompanied by an optimization strategy, e.g., considering a multiscale approach, using a large step ($\sim$5 m) to identify the main shift direction, followed with a more local search with a smaller search window and smaller shift step to refine the optimal position. Moreover, as stated in Section III-A, the flow accumulation map value at the optimal Δ_{opt} position can be interpreted as an indicator of GeoGEDI's reliability. The lower the accumulation value of Δ_{opt}, the higher the ambiguity around Δ_{opt}. Examples of low confidence footprints can be found in Fig. 11 in Appendix B. A simple threshold could be used and added to each footprint by adding a tag, warning users about possible convergence issues, similarly to quality and degrade flag implemented by NASA.

VI. Conclusion

GEDI footprints provide large scale and high sampling density data about forest structure. But low georeferencing accuracy can be detrimental to their use for predictive models of forest attributes. The proposed method is based on GEDI ground elevations and a high-resolution DEM, to improve geolocation of GEDI footprints. The method was tested on GEDI v1 and v2 for two French forests, broadleaved-dominated forest in a flat area and dense coniferous-dominated forest in a mountainous area. Our results quantified the georeferencing improvements undertaken by NASA between version 1 and 2. Besides, a ground detection issue was identified for GEDI v2 footprints using algorithm 02. However, GeoGEDI successfully improved GEDI v1 and v2 footprints positioning, simultaneously reducing bias and improving precision components. Despite improved footprint geolocation in GEDI v2, already corrected for the systematic error components, there is room for additional improvement. Yet, its performance depends on the topography, with lack of convergence in very flat areas. The method showed efficient to correct for ISS attitude and altitude variations for a diversity of forest environments, and to assess GEDI data quality with more confidence. The methods' relative simplicity allows for fast and efficient large-scale deployment, wherever a high-resolution DEM is available. With improvements in the range of those obtained with more complex methods based on waveform processing, the method is a good alternative candidate to process GEDI data prior to implementing methods requiring a precise matching of data sources, such as for data fusion purposes.

Appendix A
GEDI Ground Elevation Estimations by Selected Ground Peak Algorithm

See Table V.

TABLE V
GEDI Ground Elevation Errors for Five Footprint Groups, by Study Site

	Landes						Vosges					
Group	**% of version**	**ME**	**sdE**	**MAE**	**sdAE**	**RMSE**	**% of version**	**ME**	**sdE**	**MAE**	**sdAE**	**RMSE**
v1	100	–0.41	1.44	0.81	1.26	1.50	100	–1.19	6.34	3.90	5.14	6.45
v2 algo 01	87.4	–0.48	0.78	0.62	0.68	0.92	65.0	–0.69	2.44	1.42	2.11	2.54
v2 algo 02	12.6	0.80	3.11	2.06	2.47	3.22	35.0	0.75	5.10	3.54	3.74	5.15
v2 algo 02 pb	3.4	4.42	3.50	4.97	2.68	5.64	13.7	2.07	5.96	4.87	4.01	6.31
v2 algo 02 valid	9.2	–0.52	1.48	0.99	1.22	1.57	21.3	–0.10	4.24	2.68	3.29	4.24

The groups are: (v1) v1 footprints, (v2 algo 01) v2 footprints using ground peak algorithm 01, (v2 algo 02) v2 footprints using ground peak algorithm 02, (v2 algo 02 pb) v2 footprints using ground peak algorithm 02 where ground elevation difference between v1 and v2 is greater than 1.5 m, (v2 algo02 valid) v2 footprints using ground peak algorithm 02 where ground elevation difference between v1 and v2 is lower or equal to 1.5m. Group v2 algo 02 pb referes to footprints for which a bias was identified using algorithm 02. Group v2 algo 02 valid is the complement to the biased v2 algo 02 pb. For each group the percentage of concerned footprints is noted and GEDI ground elevation is compared to DEMref. Mean Error (ME), standard deviation of error (sdE), Mean Absolute Error (MAE), standard deviation of absolute error (sdAE) and Root Mean Square Error (RMSE) of ground elevation are shown.

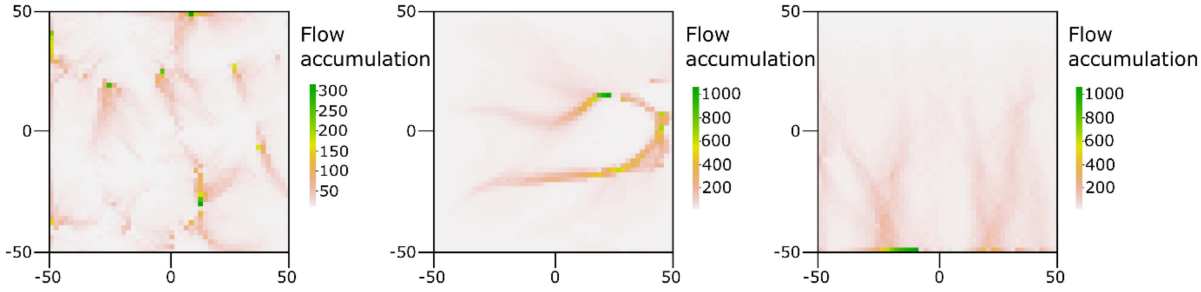

Fig. 11. Flow accumulation error maps with low maximum flow accumulation values.

Appendix B
Flow Accumulation Error Maps of the Georeferencing Method

See Fig. 11.

Appendix C
Available Dataset and Script

The dataset processed for this article is available online [44]. GEDI footprints with coordinates of unchanged GEDI v1 and v2 releases and the coordinates calculated with GeoGEDI algorithm, as well as all variables used for this article, are included.

GeoGEDI R script is available on Github [45].

Acknowledgment

We would like to thank IGN for providing the high-resolution DHM and DEM data and the GEDI mission science team for the public availability of GEDI data and their continuous work on GEDI.

References

[1] P. Potapov et al., "Mapping global forest canopy height through integration of GEDI and Landsat data," *Remote Sens. Environ.*, vol. 253, Nov. 2020, Art. no. 112165, doi: 10.1016/j.rse.2020.112165.

[2] R. Dubayah et al., "The Global Ecosystem Dynamics Investigation: High-resolution laser ranging of the Earth's forests and topography," *Sci. Remote Sens.*, vol. 1, Jun. 2020, Art. no. 100002, doi: 10.1016/j.srs.2020.100002.

[3] W. Qi, S. Saarela, J. Armston, G. Ståhl, and R. Dubayah, "Forest biomass estimation over three distinct forest types using TanDEM-X InSAR data and simulated GEDI lidar data," *Remote Sens. Environ.*, vol. 232, Oct. 2019, Art. no. 111283, doi: 10.1016/j.rse.2019.111283.

[4] J. Beck, S. Luthcke, M. Hofton, and J. Armston, "Global ecosystem dynamics investigation (GEDI) level 1B user guide. Document version 1.0," USGS Earth Resources Observation and Science (EROS) Center: NASA's Land Processes Distributed Active Archive Center (LP DAAC), Jan. 2020. [Online]. Available: https://lpdaac.usgs.gov/documents/590/GEDIL01_User_Guide_V1.pdf

[5] S. Luthcke, T. Rebold, T. Thomas, and R. Pennington, "Algorithm theoretical basis document (ATBD) for GEDI waveform geolocation for L1 and L2 products. Document version 1.0," Goddard Space Flight Center, Greenbelt, MD: NASA's Land Processes Distributed Active Archive Center (LP DAAC), Dec. 2019. [Online]. Available: https://lpdaac.usgs.gov/documents/579/GEDI__WFGEO_ATBD_v1.0.pdf

[6] C. Dou, X. Zhang, H. Guo, C. Han, and M. Liu, "Improving the geolocation algorithm for sensors onboard the ISS: Effect of drift angle," *Remote Sens.*, vol. 6, no. 6, pp. 4647–4659, Jun. 2014, doi: 10.3390/rs6064647.

[7] J. Beck, B. Wirt, S. Luthcke, M. Hofton, and J. Armston, "Global ecosystem dynamics investigation (GEDI) level 1B user guide. Document version 2.0," USGS Earth Resources Observation and Science (EROS) Center: NASA's Land Processes Distributed Active Archive Center (LP DAAC), Apr. 2021. [Online]. Available: https://lpdaac.usgs.gov/documents/987/GEDI01B_User_Guide_V2.pdf

[8] D. P. Roy, H. B. Kashongwe, and J. Armston, "The impact of geolocation uncertainty on GEDI tropical forest canopy height estimation and change monitoring," *Sci. Remote Sens.*, vol. 4, Dec. 2021, Art. no. 100024.

[9] S. Saarela et al., "Effects of positional errors in model-assisted and model-based estimation of growing stock volume," *Remote Sens. Environ.*, vol. 172, pp. 101–108, Jan. 2016, doi: 10.1016/j.rse.2015.11.002.

[10] L. Duncanson et al., "Biomass estimation from simulated GEDI, ICESat-2 and NISAR across environmental gradients in Sonoma County, California," *Remote Sens. Environ.*, vol. 242, Jun. 2020, Art. no. 111779, doi: 10.1016/j.rse.2020.111779.

[11] L. Duncanson et al., "Aboveground biomass density models for NASA's Global Ecosystem Dynamics Investigation (GEDI) lidar mission," *Remote Sens. Environ.*, vol. 270, 2022, Art. no. 112845.

[12] N. Lang, N. Kalischek, J. Armston, K. Schindler, R. Dubayah, and J. D. Wegner, "Global canopy height regression and uncertainty estimation from GEDI LIDAR waveforms with deep ensembles," *Remote Sens. Environ.*, vol. 268, Jan. 2022, Art. no. 112760.

[13] C. Silva et al., "Fusing simulated GEDI, ICESat-2 and NISAR data for regional aboveground biomass mapping," *Remote Sens. Environ.*, vol. 253, Jan. 2021, Art. no. 112234.

[14] M. Adam, M. Urbazaev, C. Dubois, and C. Schmullius, "Accuracy assessment of GEDI Terrain elevation and canopy height estimates in European temperate forests: Influence of environmental and acquisition parameters," *Remote Sens.*, vol. 12, no. 23, Jan. 2020, Art. no. 3948.

[15] I. Dorado-Roda et al., "Assessing the accuracy of GEDI data for canopy height and aboveground biomass estimates in Mediterranean forests," *Remote Sens.*, vol. 13, Jun. 2021, Art. no. 2279.

[16] J. Guerra-Hernández and A. Pascual, "Using GEDI lidar data and airborne laser scanning to assess height growth dynamics in fast-growing species: A showcase in Spain," *Forest Ecosyst.*, vol. 8, no. 1, Feb. 2021, Art. no. 14.

[17] A. Liu, X. Cheng, and Z. Chen, "Performance evaluation of GEDI and ICESat-2 laser altimeter data for terrain and canopy height retrievals," *Remote Sens. Environ.*, vol. 264, Oct. 2021, Art. no. 112571.

[18] M. Urbazaev et al., "Accuracy assessment of terrain and canopy height estimates from ICESat-2 and GEDI LiDAR missions in temperate and tropical forests: First results," in *Proc. Silvilaser*, 2021, pp. 213–215, doi: 10.34726/wim.1984.

[19] M. Milenković et al., "Influence of footprint size and geolocation error on the precision of forest biomass estimates from space-borne waveform LiDAR," *Remote Sens. Environ.*, vol. 200, pp. 74–88, Oct. 2017.

[20] C. Wang et al., "Factors affecting relative height and ground elevation estimations of GEDI among forest types across the conterminous USA," *GISci. Remote Sens.*, vol. 59, pp. 975–999, Dec. 2022, doi: 10.1080/15481603.2022.2085354.

[21] E. Quirós, M.-E. Polo, and L. Fragoso-Campón, "GEDI elevation accuracy assessment: A case study of southwest Spain," *IEEE J. Sel. Topics Appl. Earth Observ. Remote Sens.*, vol. 14, pp. 5285–5299, May 2021, doi: 10.1109/JSTARS.2021.3080711.

[22] J. Blair and M. Hofton, "Modeling laser altimeter return waveforms over complex vegetation using high-resolution elevation data," *Geophys. Res. Lett.*, vol. 26, no. 16, pp. 2509–2512, Feb. 1999, doi: 10.1029/1999GL010484.

[23] S. Hancock et al., "The GEDIsimulator: A large-footprint waveform lidar simulator for calibration and validation of spaceborne missions," *Earth Space Sci.*, vol. 6, no. 2, pp. 294–310, 2019, doi: 10.1029/2018EA000506.

[24] N. Ilangakoon et al., "Airborne and spaceborne lidar reveal trends and patterns of functional diversity in a semi-arid ecosystem," *Frontier Remote Sens.*, vol. 2, Nov. 2021, Art. no. 743320.

[25] W. Ni, Z. Zhang, and G. Sun, "Assessment of slope-adaptive metrics of GEDI waveforms for estimations of forest aboveground biomass over mountainous areas," *J. Remote Sens.*, vol. 2021, pp. 1–17, Aug. 2021.
[26] "Sylvoécorégion," IGN. [Online]. 2022. Accessed: Nov. 4, 2022. Available: https://inventaire-forestier.ign.fr/spip.php?article773
[27] M. Hofton and J. B. Blair, "Algorithm theoretical basis document (ATBD) for GEDI transmit and receive waveform processing for L1 and L2 products, Document version 1.0,," *Goddard Space Flight Center*, Greenbelt, MD: NASA's Land Processes Distributed Active Archive Center (LP DAAC), Dec. 2019. [Online]. Available: https://lpdaac.usgs.gov/documents/581/GEDI_WF_ATBD_v1.0.pdf
[28] R. Dubayah, M. Hofton, J. Blair, J. Armston, H. Tang, and S. Luthcke, "GEDI L2A elevation and height metrics data global footprint level V001," distributed by NASA EOSDIS Land Processes DAAC, 2020. [Online]. Available: https://doi.org/10.5067/GEDI/GEDI02_A.001
[29] R. Dubayah, M. Hofton, J. Blair, J. Armston, H. Tang, and S. Luthcke, "GEDI L2A elevation and height metrics data global footprint level V002," distributed by NASA EOSDIS Land Processes DAAC, 2021. [Online]. Available: https://doi.org/10.5067/GEDI/GEDI02_A.002
[30] "RGE Alti," distributed by IGN. 2022. Accessed: Nov. 4, 2022. [Online]. Available: https://geoservices.ign.fr/rgealti
[31] "RGE ALTI version 2 Descriptif de contenu," IGN. 2022. Accessed: Nov. 4, 2022. [Online]. Available: https://geoservices.ign.fr/sites/default/files/2021-07/DC_RGEALTI_2-0.pdf
[32] E. Rupnik, M. Daakir, and M. P. Deseilligny, "MicMac–A free, open-source solution for photogrammetry," *Open Geospatial Data, Softw. Standards*, vol. 2, no. 1, Jun. 2017, Art. no. 14, doi: 10.1186/s40965-017-0027-2.
[33] "BD Forêt version 2," distributed by IGN. 2022. Accessed: Nov. 4, 2022. [Online]. Available: https://geoservices.ign.fr/bdforet
[34] "RAF18", distributed by IGN. 2022. Accessed: Nov. 4, 2022. [Online]. Available: https://geodesie.ign.fr/index.php?page=grilles
[35] E. Nelson, "An examination of anticipated G-jitter on space station and its effects on materials processes," 1994. [Online]. Available: https://ntrs.nasa.gov/citations/19950006290
[36] P. Brown and A. Engelmann, "Tsis experiences with ISS jitter from inception to on-orbit operation," 2019. [Online]. Available: https://ntrs.nasa.gov/citations/20190000637
[37] T. G. Freeman, "Calculating catchment area with divergent flow based on a regular grid," *Comput. Geosci.*, vol. 17, pp. 413–422, Dec. 1991, doi: 10.1016/0098-3004(91)90048-I.
[38] Q. Wu and A. Brown, "whitebox': 'WhiteboxTools' R frontend," R package version 2.2.0, 2022. [Online]. Available: https://CRAN.R-project.org/package=whitebox
[39] J. B. Lindsay, "Whitebox GAT: A case study in geomorphometric analysis," *Comput. Geosci.*, vol. 95, pp. 75–84, 2016, doi: 10.1016/j.cageo.2016.07.003.
[40] M. Schindewolf, C. Bornkampf, M. von Werner, and J. Schmidt, "Simulation of reservoir siltation with a process-based soil loss and deposition model," *Earth Planet. Sci.*, vol. 10, pp. 41–57, 2015, doi: 10.5772/61576.
[41] B. Heung, L. Bakker, M. Schmidt, and S. Dragicevic, "Modelling the dynamics of soil redistribution induced by sheet erosion using the Universal Soil Loss Equation and cellular automata," *Geoderma*, vol. 202, pp. 112–125, Jul. 2013, doi: 10.1016/j.geoderma.2013.03.019.
[42] P. Quinn, K. Beven, P. Chevallier, and O. Planchon, "The prediction of hillslope flow paths for distributed hydrological modelling using digital terrain models," *Hydrol. Process.*, vol. 5, no. 1, pp. 59–79, Jan. 1991, doi: 10.1002/hyp.3360050106.
[43] D. Guyon, S. Laventure, T. Belouard, J.-C. Samalens, and J.-P. Wigneron, "Retrieving the stand age from a retrospective detection of multinannual forest changes using landsat data. Application on the heavily managed maritime pine forest in Southwestern France from a 30-year landsat time-series (1984-2014)," in *Proc. IEEE Int. Geosci. Remote Sens. Symp.*, 2015, pp. 1968–1971, doi: 10.1109/IGARSS.2015.7326182.
[44] A. Schleich, S. Durrieu, M. Soma, and C. Vega, "GEDI footprints with corrected geolocation with DEM," Recherche Data Gouv, Apr. 2023, doi: 10.57745/EJ4CI3.
[45] A. Schleich, "GeoGEDI," Apr. 2023. [Online]. Available: https://github.com/aschleich/GeoGEDI

Anouk Schleich received the M.Sc. degree in geomatics engineering from the École Nationale des Sciences Géographiques, Marne-la-Vallée, France, in 2020. She is currently working toward the Ph.D. degree in geomatics with the INRAE Montpellier, Montpellier, France.

Her research interests include lidar and forest inventory.

Sylvie Durrieu received the M.Sc. degree in forest and plant biology from the University of Nancy, Nancy, France, in 1989, and the engineering degree in forestry and the Ph.D. degree in remote sensing from the French Institute of Forestry, Agricultural and Environmental Engineering, Paris, France, in 1989 and 1994, respectively.

She obtained an accreditation to supervise research in Earth and Water Sciences from the University of Montpellier, Montpellier, France, in 2018. From 1994 to 1999, she worked with the French National Forest Inventory and carried out R&D in the field of remote sensing applied to forest inventory and mapping, focusing on optical imagery technology. Since 1999, she has been working with IRSTEA then INRAE. She has developed methods for characterizing and monitoring forest resources and biodiversity from 3-D LiDAR data. She was a PI of LEAF (LiDAR for Earth and Forests), a project of space LiDAR mission submitted to ESA in 2008, and supported by CNES from 2013 to 2020 as a potential mid-term space mission. Her research interests include LiDAR technology for forest ecosystem monitoring.

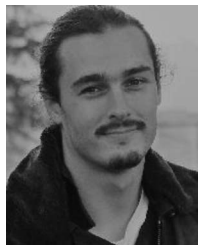

Maxime Soma received the M.S. degree in forestry, agronomy and ecosystems management (speciality forests and their environment) from the AgroParisTech, Nancy, France, in 2015, and the Ph.D. degree in environmental science from the University of Aix-Marseille, Aix-en-Provence, France and the French Institute for Agricultural Research and Environment (INRAE), France, in 2019.

From 2016 to 2021, he worked as Ph.D. Student and a Postdoctoral Fellow with the INRAE on light detection and ranging (LiDAR) data processing for forests and crops 3-D structure measurements. From 2021 to 2022, he benefited from a postdoctoral scholarship of the Centre National d'Etudes Spatiales for investigating the potential of spaceborne LiDAR instruments for national forest inventory within UMR TETIS (INRAE). He is currently working as a Researcher with the UMR RECOVER, Aix-en-Provence, France. His research interests include application of remote sensing technologies for fire risk monitoring.

Cédric Vega received the master's degree in ecology from the Paul Sabatier University, Toulouse, France, in 2000, and the Ph.D. degree in environmental sciences from the UQAM, Montréal, QC, Canada, in 2006.

He obtained the Accreditation to supervise research (HDR) in Ecology from the Paul Sabatier University, in 2017. From 2010 to 2014, he headed the Laboratory of Applied Informatics and Geomatics, Institut Français de Pondichéry, Pondicherry, India. He is currently a Senior Researcher with the ENSG, National Institute of Geographic and Forest Information, Laboratory of Forest Inventory, Nancy, France. His research interests include remote sensing of forest ecosystems, particularly using LiDAR, photogrammetry, and high-resolution optical imagery. He is particularly focusing on developing methods for both quantifying forest structures and dynamics, and estimating forest biophysical parameters.